

Augmenting Perceptual Super-Resolution via Image Quality Predictors

Fengjia Zhang*

Samrudhdhi B. Rangrej*

Tristan Aumentado-Armstrong*

Afsaneh Fazly Alex Levenshtein

AI Center – Toronto, Samsung Electronics

{f.zhang2, s.rangrej, tristan.a, a.fazly, alex.lev}@samsung.com

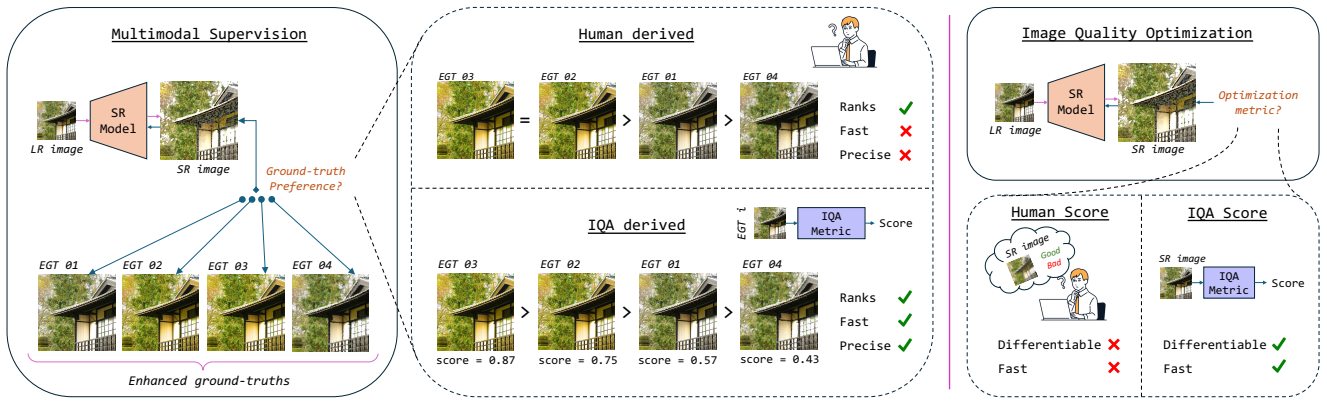


Figure 1. **Schematics for improving perceptual super-resolution (SR).** Perceptual quality of SR can be improved in two ways: (**Left**) providing supervision through multiple enhanced ground-truths (EGT) or (**Right**) direct optimization for the quality of the super-resolved image. In both cases, human-in-the-loop can greatly improve performance. However, manual annotation is tedious, imprecise, and non-differentiable. An IQA metric can replace a human in rating the enhanced ground-truths or can directly act as a differentiable optimization objective. In this paper, we specifically assess whether more practical no-reference (NR) IQA metrics can replace human raters for SR. We find that combining NR-IQA-based sampling and regularized optimization is sufficient to attain state-of-the-art perceptual image quality, *without* requiring human ratings.

Abstract

Super-resolution (SR), a classical inverse problem in computer vision, is inherently ill-posed, inducing a distribution of plausible solutions for every input. However, the desired result is not simply the expectation of this distribution, which is the blurry image obtained by minimizing pixelwise error, but rather the sample with the highest image quality. A variety of techniques, from perceptual metrics to adversarial losses, are employed to this end. In this work, we explore an alternative: utilizing powerful non-reference image quality assessment (NR-IQA) models in the SR context. We begin with a comprehensive analysis of NR-IQA metrics on human-derived SR data, identifying both the accuracy (human alignment) and complementarity of different metrics. Then, we explore two methods of applying NR-IQA models to SR learning: (i) altering data sampling, by building on an existing multi-ground-truth SR framework, and (ii) directly optimizing a differentiable quality score.

Our results demonstrate a more human-centric perception-distortion tradeoff, focusing less on non-perceptual pixel-wise distortion, instead improving the balance between perceptual fidelity and human-tuned NR-IQA measures.

1. Introduction

Many tasks in human and computer vision are naturally formulated as ill-posed inverse problems [65]. Single-image super-resolution (SISR), which has many practical applications to digital photographic zoom, is a well-studied example of this (e.g., [4, 24]). In SISR, a given low-resolution (LR) image has an associated distribution of high-resolution (HR) “real” images that could have given rise to it. The fundamental challenge of SR is therefore not just to find *any* sample from that distribution, but instead to find perceptually plausible one(s). Early learning-based models, trained with pixel-wise losses (e.g., [21, 22]), effectively “average” over possible solutions in pixel-space, resulting in

*Equal Contribution.

blurry output images with a high peak signal-to-noise ratio (PSNR). However, human preferences indicate that a solution with high image quality is better than this averaged one. Hence, numerous techniques have been devised to emphasize perceptual fidelity, such as perceptual metrics [19, 39] and adversarial losses (e.g., [70]), greatly improving image quality. In other words, pixelwise fidelity is a poor measure of perceptual quality. In fact, under some conditions, they are directly oppositional, forming a “perception–distortion tradeoff” [5, 6]. In theory, the only pixel-space constraint is given by the LR image; besides this, the optimal SR result (in terms of human preference) may have very high pixelwise distortion (w.r.t. the “real” ground-truth generating image), as long as it has high plausibility with respect to the LR input and high image quality.

Instead of optimizing pixel-space distortions, we focus on improving perceptual image quality. This is commonly done using a combination of perceptual losses and GANs [48, 58, 61, 79, 84], enabling the SR model to target a multi-modal distribution rather than specific ground-truth targets. The challenge of such methods, however, is to produce perceptually plausible outputs without introducing high-frequency artifacts [51]. Many full-reference (FR) [18, 27, 42, 99] and non-reference image quality assessment (NR-IQA) [41, 68, 74, 75] metrics were developed to align with human preferences for identifying perceptually plausible images. While some approaches started to replace perceptual losses with FR metrics like LPIPS [42] and DISTS [18], for the task of image restoration, NR-IQA metrics are still used purely for evaluation purposes. Motivated by the adoption of human feedback guidance in text-to-image generative models (e.g., [16, 23, 67, 92]), we aim to use NR-IQA metrics to improve SISR.

Recently, Chen et al. [12] used human feedback to improve SISR. They do so by generating multiple enhanced versions of GT (Fig. 1 left), manually rating these different versions using multiple human evaluators, and fine-tuning the model on the positively ranked GTs. While this results in significant perceptual quality improvements without introducing unwanted artifacts, manual human ranking is very coarse and cumbersome. We instead use an automatic NR-IQA measure that is well-correlated with human scores, yielding a more fine-grained ranking, and bypassing the requirement for having human feedback (Fig. 1 centre). Additionally, since the measure is fully differentiable, it can be used for direct optimization (e.g., replacing or complementing GANs), unlike human scores that cannot be used in this fashion (Fig. 1 right). Our contributions are as follows:

- We present a detailed analysis of NR-IQA on two human-derived SR datasets, thus identifying metrics that are generally useful for improving SR image quality.
- We explore the application of NR-IQA to SISR, via two approaches: sampling across multiple GTs weighted by

NR-IQA, and direct optimization of NR-IQA.

- We achieve SISR results that are perceptually on par or better than SISR finetuned with human feedback, but using an automatic NR-IQA measure instead.

2. Related Work

Deep learning-based SISR: Deep learning has given a significant boost to SISR performance, taking the SOTA mantle from dictionary-based methods [76, 77, 93] to CNN-based approaches like SRNet and its successors [2, 21, 22, 44]. Since then, there came many architectural improvements: deeper architectures, like RCAN [102], hierarchical processing [47], advanced building blocks like in NAFNet [13] and RRDB from ESRGAN [84], and better upsampling like PixelUnshuffle [71], to name a few. Due to long range dependencies in SISR, transformer-based methods [14, 50], and auto-regressive models based on Mamba [54], have recently achieved SOTA performance [15, 32].

Perceptual quality-oriented SISR: Early SISR approaches optimized a simple pixel-wise reconstruction loss, such as L2 or L1, between model output and ground-truth [21, 22]. However, due to the ill-posedness of SISR, this yields poor perceptual quality. Blau and Michaeli [6] have shown that there exists a tradeoff between good perceptual quality and accurate reconstruction (or fidelity). To improve perceptual quality, perceptual losses were proposed, such as SSIM [86], which measures patch similarity rather than per-pixel similarity, and later others [39] that measure the similarity between deep VGG features rather than pixel intensities. Combined with perceptual losses, GAN-based training [30] was used to improve perceptual quality in SRGAN [48] and many follow-up approaches [3, 58, 61, 79, 84]. One challenge of such approaches is to improve perceptual quality without introducing unwanted hallucinations. Proposed solutions include more specialized discriminators [62] and better balancing between various loss terms [51, 63]. Rather than changing the training loss function, perceptual quality can be improved by explicitly generating multiple training targets [12, 38], or encouraged using specific architectural designs. Normalizing flows [56, 96] were used to directly output a distribution over plausible solutions rather than a single SR image. More recently, diffusion-based approaches [40, 69, 83, 89–91, 95] and alike [17] have been shown to achieve a better perceptual quality than GAN-based methods.

Human guided perceptual quality assessment: One may use image quality assessment (IQA) metrics to evaluate the aesthetic quality of super-resolved images. They can be full-reference (FR) or no-reference (NR) metrics. In real-world applications where the true HR image is unavailable, NR-IQA metrics are more useful. Early opinion-unaware NR-IQA metrics used hand-crafted features to assess how closely the statistics of the output images match with nat-

Method	PaQ-2-PiQ [97]	NIMA [†] [74]	MUSIQ [‡] [41]	LIQE [♡] [101]	ARNIQA-TID* [1]	Q-Align [△] [88]	TOPIQ-NR [11]
Accuracy (%)	76.41	74.91	74.47	74.03	74.03	73.77	73.06

Table 1. **Phase I analysis on SBS180K.** Accuracy of top 7 NR-IQA metrics on a subset (1212 image pairs) from train portion. We use the default configuration of the metrics, provided by the IQA-PyTorch toolbox, unless stated otherwise. [†]We use NIMA with Inception V2 as base model. [‡]We use the default MUSIQ trained on KonIQ [35]. [♡]We use LIQE pretrained on KonIQ [35]. *We use ARNIQA metric trained on TID2013 [66]. [△]We use Q-Align metric specialized in image quality assessment.

Method	PaQ-2-PiQ [97]	NIMA [†] [74]	MUSIQ [‡] [41]	LIQE [♡] [101]	ARNIQA-TID* [1]	Q-Align [△] [88]	TOPIQ-NR [11]
Train Acc. (%)	80.41	79.32	79.96	77.70	77.74	80.00	78.30
Test Acc. (%)	80.57	81.37	82.73	77.45	77.07	80.68	81.28

Table 2. **Phase II analysis on SBS180K dataset.** Accuracy of top 7 (according to Phase I) NR-IQA metrics on the entire train and test sets of SBS180K. We exclude image pairs where humans prefer both images equally. ^{†‡♡△} See Table 1.

ural scene statistics, e.g., BRISQUE [59] and NIQE [98]. Others developed metrics that align with human preferences [68, 75]. Recently, many developed deep-learning-based opinion-unaware approaches such as FID [34], and opinion-aware approaches such as NIMA [74] and MUSIQ [41]. While the above metrics are general purpose, metrics such as NRQM [57] and NeuralSBS [43] are specifically designed to align with human preferences for super-resolution. Recently, human preferences are being widely incorporated in improving generative models, especially for text-to-image generation [16, 52, 92]. Yet, incorporating human guidance in improving SR models has not received much attention. Ding *et al.* [19] attempt to use various *full-reference* IQA metrics for SR model finetuning, and Chen *et al.* [12] propose to use *human guidance in GT selection process*. Unlike these works, we attempt to assess the ability of *no-reference* IQA metrics to (a) automatically rate and select optimal GT, eliminating the need for arduous manual annotation, and (b) act as a finetuning objective to improve aesthetic quality of super-resolved images.

3. Analysis of NR-IQA metrics

We analyze the alignment between various NR-IQA metrics and human judgements for assessing the aesthetic quality of super-resolved images. We report our analysis on two publicly available datasets, SBS180K [43] and HGGT [12].

3.1. Analysis on the SBS180K dataset

We analyze various NR-IQA metrics on SBS180K [43], a large scale human preference dataset for super-resolved images, containing 167,019 train and 9,421 test image pairs. Each pair is annotated with a single score in the range [0,1], depicting the fraction of human annotators preferring the aesthetic quality of the second image over the first one. Each pair consists of two super-resolved versions of the same low-resolution image, with each version generated using a different SR model. Due to the large size of SBS180K,

we analyze the metrics in two phases. In phase I, we analyze 20 NR-IQA metrics and their variants (total 42 metrics) on a small subset of the train set. In phase II, we analyze the top 7 NR-IQA metrics from phase I on the complete train and test sets. We use IQA-PyTorch[10], an open-source toolbox for image quality assessment.

Phase I. There are 404 unique pairs of compared SR models in the train set. We randomly select 3 image pairs per model comparison, yielding a subset of 1212 images. We evaluate the following NR-IQA metrics on this subset: Q-Align [88], LIQE [101], ARNIQA [1], TOPIQ [11], TReS [29], CLIP-IQA(+) [82], MANIQA [94], MUSIQ [41], DBCNN [100], PaQ-2-PiQ [97], HyperIQA [72], NIMA [74], WaDIQaM [8], CNNIQA [104], NRQM [57], PI (Perceptual Index) [7], BRISQUE [59], ILNIQE and NIQE [98], and PIQE [81]. When available, we also consider multiple variants of these metrics offered by IQA-PyTorch (e.g., metrics trained on different IQA datasets). We assess the accuracy of each metric in terms of whether, given an image-pair, the metric prefers the same image as the humans prefer collectively or not. Table 1 shows results of only the top 7 metrics: PaQ-2-PiQ, NIMA, MUSIQ, LIQE, ARNIQA, Q-Align, TOPIQ-NR. Complete results are given in Supp. Table 6.

Phase II. We evaluate the top 7 metrics from Phase I on the complete train and test sets, excluding pairs with no consensus among human annotators (score of 0.5). Results are given in Table 2, suggesting that MUSIQ has relatively higher accuracy on both train and test sets compared to other metrics. While PaQ-2-PiQ and Q-Align have slightly higher accuracy (0.45% and 0.04%, respectively) on the train set, MUSIQ outperforms them on the test set by a large margin (2.16% and 2.05%, respectively). We further analyze performance of the remaining six metrics on the samples where MUSIQ fails (excluding pairs with a score of 0.5). Results are shown in Table 3. We find that NIMA and Q-Align achieve higher accuracy on these samples compared

to other four metrics. Since they complement MUSIQ, in §5, we report performance on MUSIQ, NIMA and Q-Align.

3.2. Analysis on HGGT dataset

We analyze the seven selected metrics of Phase I above on the HGGT [12] dataset, containing 20,193 quintuplets of HR image patches. Each quintuplet contains an original HR ground-truth (GT) patch and four enhanced GTs. Each of the four enhanced GTs in each quintuplet is annotated by human annotators for being better than ('positive'), similar to ('similar'), or worse than ('negative') the original GT. While 'positive' labels are abundant, 'negative' labels are rare. Out of 20,193, only 1,270 quintuplets have at least one 'negative'. We analyze the seven metrics on this subset.

We evaluate the NR-IQA metrics based on the average Spearman rank correlation coefficient, and positive and negative misalignment rates. Assuming higher rank is better, we define positive (negative) misalignment rate as the fraction of quintuplets where at least one positive (negative) GT is ranked lower (higher) than at least one similar GT. We show results in Table 4. Note that all metrics have poor negative misalignment rate, leading to low Spearman correlations. We believe that NR-IQA metrics fail to recognize negative GTs, since they may not necessarily have low quality (recall that all are enhanced GTs), or may have artifacts that are unrecognizable without a reference image. Nonetheless, MUSIQ has the lowest positive misalignment rate. Hence, we use MUSIQ in §4 for weighted sampling of the GTs and direct optimization (see also Supp. §7.1). Since TOPIQ has the 2nd lowest positive misalignment rate after MUSIQ, we include it as an evaluation metric in §5.

4. Methods

We next explore how to improve existing SR methods with the results of our findings. Since our interest is in *perceptual* quality and its use in multimodal SR, we build upon recent work, Human Guided Ground-truth (HGGT) [12], which constructs a *set* of ground-truth images per input, with varying quality, and uses human tests to rank their relative quality. We begin by reviewing HGGT [12] (§4.1), and then discuss two methods of applying neural IQA models to augment it: altering the choice of ground-truth set based on an automated IQA weight (§4.2) and directly optimizing the IQA model in a fine-tuning step (§4.3).

4.1. Background

As discussed in §3.2, the HGGT dataset includes (i) a set of images ("originals"), (ii) a set of four super-resolved versions of each original ("enhanced GTs"), and (iii) human annotations for each enhanced GT ("positive", "similar", or "negative" meaning better than, indistinguishable from, or

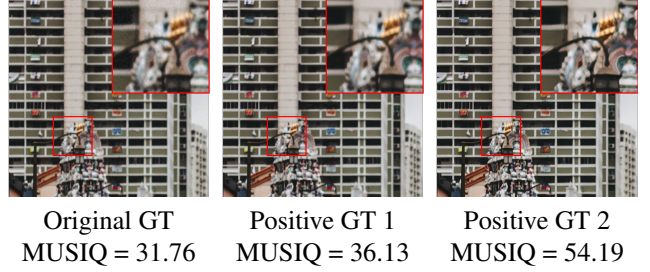


Figure 2. **Fine-Grained Comparison via NR-IQA.** MUSIQ can differentiate the quality of two images, both marked as “positive” by human annotators. Higher MUSIQ indicates higher quality (zoom for details). Unlike HGGT models, which utilize a uniform distribution over positives, our approach enables differently weighting them (§4.2).

worse than the original). The set of positives provides *multimodal* supervision, since each one is a disparate yet reasonable GT for learning. The HGGT work [12] then shows that utilizing these synthetic GTs is useful for SR training, exploring several neural architectures and degradation settings. While HGGT explores several variants for utilizing their human labels, we focus on the simple but highly performing “positives-only” scenario, which performs equivalently or better than the variants utilizing negatives. In this scenario, at each training iteration, every input image supervises the network with a GT chosen *uniformly randomly* from the positives. As is relatively standard in SR (e.g., [37, 85]), HGGT models are trained with a combined loss:

$$\mathcal{L}(\theta|\hat{I}, I) = \lambda_{\ell_1}||I - \hat{I}||_1 + \lambda_P d_P(\hat{I}, I) + \lambda_A D(\hat{I}), \quad (1)$$

where $\hat{I} = f_\theta(I_{LQ})$ is the SR estimate of the low-resolution (or low-quality) input I_{LQ} , via SR network f_θ , $I \sim \mathcal{U}_{I_{LQ}}[\{I_1, \dots, I_n\}]$ is the randomly chosen GT (from the set of positives corresponding to image I_{LQ}), d_P is a perceptual loss, and D is an adversarial discriminator.

However, HGGT requires human labels, which are difficult to scale and often domain-dependent. In contrast, we explore the opportunities afforded by neural no-reference image quality assessment (NR-IQA) models, which not only eschew human labels, but also confer additional capabilities – namely, the ability to provide more fine-grained non-uniform sampling weights (§4.2) and to enable direct optimization via differentiability (§4.3).

4.2. Reweighted Sampling

We explore a few straightforward alternatives to uniform sampling of the positives, via an IQA model. In particular, consider the following simple formulation:

$$I \sim \mathcal{P}[S_I | \text{SoftMax}_\tau(Q(S_I))], \quad (2)$$

$$Q(S_I) = \{Q(I_1), \dots, Q(I_n)\}, \quad (3)$$

$$S_I = \{I_1, \dots, I_n\} \in \{A_I, P_I\} \quad (4)$$

Method	PaQ-2-PiQ [97]	NIMA [†] [74]	LIQE [◊] [101]	ARNIQA-TID* [1]	Q-Align [◊] [88]	TOPIQ-NR [11]
Train Acc. (%)	37.58	44.21	31.50	42.05	42.86	25.71
Test Acc. (%)	33.10	39.70	30.70	38.60	41.06	30.89

Table 3. **Phase II analysis on SBS180K (continued).** Accuracy of top 6 NR-IQA metrics on consensus samples (from train plus test) where MUSIQ fails. ^{†◊*} See Table 1.

Method	PaQ-2-PiQ [97]	NIMA [†] [74]	MUSIQ [◊] [41]	LIQE [◊] [101]	ARNIQA-TID* [1]	Q-Align [◊] [88]	TOPIQ-NR [11]
SRC \uparrow	0.10	0.17	0.17	0.03	0.28	0.20	0.09
PM \downarrow	0.26	0.28	0.16	0.58	0.51	0.39	0.21
NM \downarrow	0.85	0.79	0.95	0.64	0.45	0.63	0.97

Table 4. **Analysis on HGGT subset.** We evaluate Spearman’s rank correlation coefficient (SRC), positive misalignment (PM) rate, and negative misalignment (NM) rate. ^{†◊*}. See Table 1.

where I is the sampled GT, $\tau > 0$ is the softmax temperature, Q is the NR-IQA model (higher is better), \mathcal{P} is a discrete distribution over elements of S_I (weighted by $\text{SoftMax}_\tau(Q(S_I))$), and S_I is the set of possible GTs (either choosing from *all* candidates, enhanced and original, denoted A_I , or just *positive* ones, P_I). The HGGT algorithm simply uses $S_I = P_I$ and $\tau \rightarrow \infty$ (i.e., the uniform distribution); we explore different combinations, including $\tau \rightarrow 0$ (the arg max choice). We illustrate the utility of NR-IQA-based sampling (as opposed to uniform) in Fig. 2, displaying an example that humans rank equivalently as positive, yet is more precisely distinguished by the neural assessor. We consider three NR-IQA-based sampling scenarios.

Softmax-All (SMA). Given the set of all GTs (i.e., $S_I = A_I$), we use an IQA-weighted distribution over GTs. This setting uses no human data, and simply randomly chooses a GT at each iteration with a weight proportional to softmax-rescaled quality. We set τ to ensure a distribution between uniform and Kronecker delta (i.e., argmax).

Softmax-Positives (SMP). This approach actually builds on the human data in HGGT, using the softmax-normalized IQA scores but only of the positives (i.e., $S_I = P_I$). This setting is the most similar to the HGGT positives-only (or uniform distribution on positives), just with non-uniform weights (based on τ). We expect this to outperform SMA sampling, as it has access to direct human preferences.

Argmax-online (AMO). The use of a neural IQA model confers an additional capability that human data lacks: we can dynamically determine sampling weights for new patches at training time. In previous scenarios, at training time, we first pick one GT out of the four (Eq. 3), followed by random patch sampling from the selected GT. Instead, in the Argmax-online (AMO) scenario, we first sample a random patch from each GT, followed by selecting the best patch. To be specific, we sample one patch from the same random location from each GT, then run Q on each patch, and choose the best one (i.e., the arg max of Q values, so



Figure 3. **Structured Optimization Noise.** Optimizing via an NR-IQA metric (MUSIQ [41]) generates structured artifacts (left), similar to an adversarial attack, while utilizing LoRA removes this noise (right; see §4.3 and Supp. §10.2). Zoom in for details.

$\tau \rightarrow 0$). We eschew human data; hence, $S_I = A_I$. This enables a more fine-grained judgment (since quality is computed at the *patch* level), whereas human annotations cannot necessarily be so easily extrapolated.

4.3. Direct Optimization

Given a differentiable image quality estimator, Q , an obvious approach to improving our SR model is to simply include Q in our objective function. To some extent, this has already been explored for unconditional generative models (e.g., [16]). However, when Q is a neural network with many parameters, this is unlikely to succeed; in essence, gradient descent will act like an “adversarial attack” on Q (e.g., [31]). It is well-known that such “attacks” are often able to dramatically alter the output of the objective network (say, a classifier), while changing the optimized input in unintuitive or imperceptible ways (e.g., [45, 73]); in SR, this could conceivably manifest as artifacts that fool Q into providing a high score, since NR-IQA models are known to be susceptible to attacks (e.g., [33, 55]). In fact, without additional regularization, this is precisely what happens: in Fig. 3, we display the artifacts that appear when an SR network is naively fine-tuned with Q (see also Supp. §10.2).

Thus, inspired by prior work [16], we utilize low-rank adaptation (LoRA) [36] to regularize the optimization. Formally, we continue training as normal, but only on the LoRA weights, plus an additional NR-IQA loss term:

$$\tilde{\mathcal{L}}(\phi|\hat{I}, I) = \mathcal{L}(\phi|\hat{I}, I) - \lambda_Q Q(\hat{I}), \quad (5)$$

where ϕ are the LoRA parameters, $\hat{I} = f_{\theta, \phi}(I_{LQ})$, Q is an NR-IQA model (where higher is better), and \mathcal{L} is defined in Eq. 1. Unless otherwise specified, we set $\lambda_A = 0$ when fine-tuning, since we are already including an image quality term (for which the critic normally acts; though see §5.2). See Supp. §8 for additional details.

5. Experiments

Setup. We consider the HGGT dataset under two degradation settings for the super-resolution (SR) problem: (a) the standard Real-ESRGAN scenario (two random degradation rounds) [85] and (b) a simplified setting with a single round, used in the HGGT paper. We use the ESRGAN (RRDB-based) architecture [84, 85] for (a) and SwinIR [50] for (b). Unless otherwise stated, we use the same training settings as HGGT. Based on our analysis in §3, unless noted otherwise, we use MUSIQ [41] as our NR IQA model, Q , for both weighted sampling and direct optimization.

Evaluation. Following HGGT [12], we utilize their Test-100 held-out images for evaluation. We utilize two low-level distortion metrics, PSNR and SSIM [86]. We also use three FR models, which act as mid-level visual metrics: LPIPS [102], LPIPS-ST [28], and DIST [20]. LPIPS-ST [28] is a *shift-tolerant* form of LPIPS [102], improving robustness to small translations imperceptible to humans but highly damaging to distortion measures. Finally, we apply four NR-IQA metrics. Since we are interested in differentiating high-quality images, we choose MUSIQ [41] and TOPIQ [11] as they have the best positive misalignment scores (see Table 4). We also include NIMA [74] and Q-Align [88] based on their complementarity with MUSIQ (see §3.1), which is directly optimized. Since Test-100 has multiple positive GTs per image, evaluations with reference-based metrics are averaged across all positives.

Baselines. We compare to the SOTA “positives-only” model for HGGT, which we denote UPos, as it uses a uniform distribution over positive samples. We include two human-annotation-free baselines that do not incorporate NR-IQA: “OrigsOnly”, which trains only with original (non-enhanced) GT, and “Rand”, which randomly chooses a supervisory image from among *all* potential GTs. For our methods, we can choose (a) an IQA-based sampling type and (b) IQA-based fine-tuning settings. The different sampling methodologies (SMA, SMP, and AMO) are described in §4.2, while we denote the use of fine-tuning (see §4.3) with the “FT” moniker. We also consider two main FT variations, FT_{IG} and FT_{HP} , described in §5.2. Our primary method combines the best settings for both IQA-based sampling and optimization: the AMO+FT scheme.

5.1. Empirical Results

Our results on HGGT Test-100 are displayed in Table 5 and Fig. 4. See Supp. §11 for RealSR results as well.

Multimodal Training Boosts Performance. As in HGGT, we can see the impact of enhanced GTs by comparing Orig-*sOnly* to UPos, which has greatly improved perceptual quality (LPIPS, DIST, and NR-IQA). We also consider the Rand baseline, showing that even randomly sampling enhanced GTs is helpful for perceptual quality but not sufficient to reach UPos performance, the SoTA method from HGGT, enabled by *human* filtering of low-quality GTs.

Neural IQA Sampling Outperforms Human Rankings. We next investigate whether IQA-based sampling (SMA, SMP, and AMO) can outperform UPos, which relies on human rankings. On SwinIR, LPIPS and DIST remain largely unchanged, but LPIPS-ST and the NR metrics show small improvements, especially for AMO. On Real-ESRGAN, sampling with IQA improves both LPIPS and LPIPS-ST, but only AMO shows substantial improvements on the NR metrics. Surprisingly, despite access to human labels, SMP is very similar to SMA, maintaining nearly identical performance on low and mid level distortion measures, with a marginal boost in NR image quality. In general, we find AMO is consistently superior to both SMA and SMP, which suggests that selecting for quality (especially at the fine-grained level demanded in the online setting) is more important than simply having multiple GTs; AMO is also measurably better than UPos in terms of perceptual quality, despite the lack of access to human annotation.

IQA Fine-tuning Improves both Human and Neural Sampling. We examine the impact of fine-tuning (FT) on NR-IQA. When used on top of human data, denoted UPos+FT, LPIPS and DIST are the same (SwinIR) or slightly worse (RealESRGAN), but NR-IQA metrics uniformly improve, as well as, interestingly, LPIPS-ST. This trade-off of mid-level perceptual distortion for high-level quality is effectively an extension of the previously observed balance, between pixel-level distortion versus perceptual metrics. Indeed, we still see the latter compromise here, in that FT always damages low-level distortion metrics (PSNR and SSIM), despite the increases in perceptual quality. This is expected, since NR-based FT does not optimize to a particular SR solution, let alone the one(s) in the dataset. In addition, the results with LPIPS-ST indicate that it is more perceptual than LPIPS or DIST (i.e., more NR-IQA-like, though still full-reference). Overall, the performance boosts with FT suggest that useful information can be extracted from neural NR-IQA models, even on top of a model with access to human annotations, providing a simple mechanism for improving image quality in SR models.

Upper-bounding NR-IQA Evaluation Performance. In addition, we compute “gold standard” NR-IQA values for the GT Test data, taking the best score among the original and enhanced images, providing a soft upper-bound on NR scores, if one were able to exactly reproduce the “best” GT via the SR network. We find that altered sampling generally

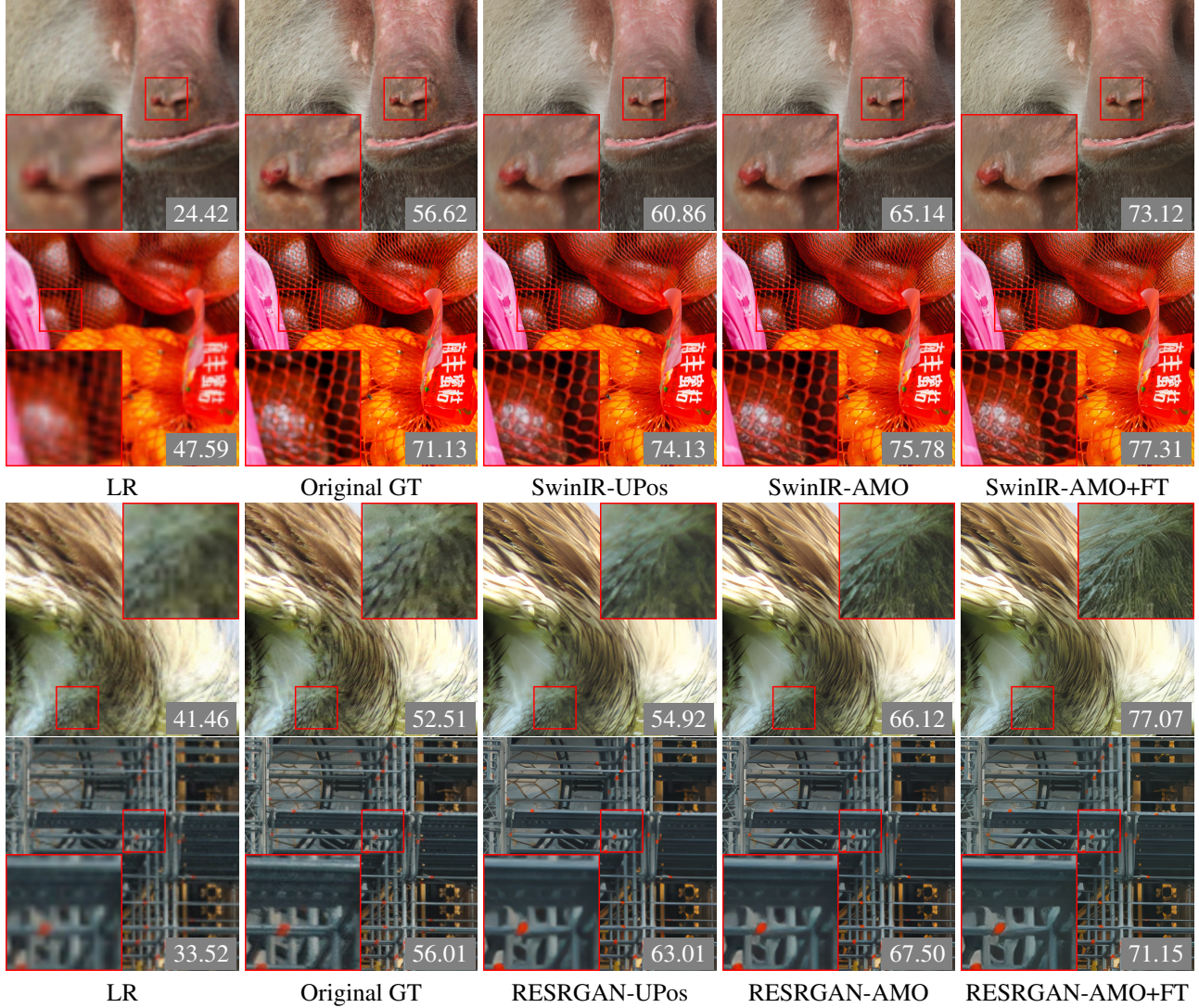


Figure 4. Qualitative results with NR-IQA Guidance. Following the notation of Table 5, columns 3-5 are (top 2 rows) SwinIR-UPos, SwinIR-AMO, and SwinIR-AMO + FT, and (bottom 2 rows) Real-ESRGAN-UPos, Real-ESRGAN-AMO, and Real-ESRGAN-AMO + FT. We show MUSIQ scores in insets. Qualitatively, we see improved performance as we move from ‘UPos’ to ‘AMO’ to ‘AMO+FT’, showcasing superiority of each method over the previous one. Zoom in for details. See also Supp. §10.1 for additional examples.

does not reach these values, but FT is able to reach and even surpass them in several scenarios.

Superior Perceptual Quality via Neural Sampling and Fine-Tuning. Finally, we test the natural unification of IQA-based neural sampling with IQA-driven FT, denoted by the AMO+FT setting. We find that this combination surpasses the SoTA HGGT approach (UPos), in terms of perceptual quality, despite *not using any human annotations*. Specifically, for SwinIR, AMO+FT incurs a small penalty ($\sim 3\text{-}4\%$) on LPIPS and DISTs, but improves LPIPS-ST by $\sim 6\%$ and is superior to every other method according to NR metrics. In the RealESRGAN setting, compared to UPos, AMO+FT again obtains a large improvement on LPIPS-ST ($\sim 12\%$), with negligible changes on the other mid-

level metrics ($\sim 2\%$). It also soundly surpasses UPos according to *every* NR metric. Interestingly, RealESRGAN-AMO+FT does not outperform RealESRGAN-UPos+FT; however, note that the latter has access to human annotations. We also present a user study in Supp. §12, finding a preference for AMO+FT over UPos. Altogether, these results suggest (i) human annotated rankings on multiple GTs, at least when used naively for SR training, can be easily surpassed via neural NR-IQA scores, and (ii) considerable improvements to the perceptual quality of SR models can be attained through automated means, by simply applying existing NR-IQA models.

Model	()	FR Low-Lev. Dist.			FR Mid-Lev. Dist.			NR High-Lev. Perceptual Quality			
		PSNR \uparrow	SSIM \uparrow	LPIPS \downarrow	LPIPS-ST \downarrow	DISTS \downarrow	MUSIQ \uparrow	NIMA \uparrow	Q-Align \uparrow	TOPIQ \uparrow	
Gold Standard	✗	–	–	–	–	–	69.64	5.28	3.78	0.69	
SwinIR-OrigsOnly	✓	22.72	0.652	0.227	0.174	0.162	59.47	4.87	3.17	0.48	
SwinIR-Rand	✓	22.45	0.650	0.180	0.139	0.131	65.27	5.11	3.52	0.59	
SwinIR-UPos*	✗	22.30	0.647	0.169	0.129	0.123	66.39	5.16	3.56	0.62	
SwinIR-SMA	✓	22.27	0.646	0.171	0.129	0.124	66.73	5.16	3.60	0.63	
SwinIR-SMP	✗	22.29	0.647	0.171	0.130	0.124	66.83	5.17	3.62	0.62	
SwinIR-AMO	✓	22.08	0.641	0.167	0.124	0.123	68.08	5.21	3.67	0.66	
SwinIR-UPos + FT _{HP}	✗	22.17	0.642	0.166	0.123	0.122	68.38	5.23	3.64	0.65	
SwinIR-UPos + FT _{IG}	✗	22.03	0.635	0.168	0.122	0.123	69.37	5.24	3.69	0.66	
SwinIR-UPos + FT	✗	22.01	0.633	0.169	0.123	0.124	69.70	5.26	3.70	0.67	
SwinIR-AMO + FT	✓	21.77	0.624	0.174	0.121	0.128	70.81	5.29	3.75	0.70	
ReSRGAN-OrigsOnly	✓	22.10	0.618	0.283	0.229	0.185	57.91	4.84	2.99	0.46	
ReSRGAN-Rand	✓	21.66	0.611	0.234	0.190	0.160	64.82	5.18	3.40	0.60	
ReSRGAN-UPos*	✗	21.54	0.608	0.233	0.192	0.158	65.93	5.25	3.47	0.63	
ReSRGAN-SMA	✓	21.46	0.606	0.227	0.182	0.157	65.87	5.23	3.46	0.63	
ReSRGAN-SMP	✗	21.44	0.607	0.226	0.182	0.156	66.66	5.24	3.51	0.64	
ReSRGAN-AMO	✓	21.28	0.602	0.224	0.178	0.156	67.86	5.29	3.56	0.66	
ReSRGAN-UPos + FT _{HP}	✗	21.30	0.595	0.226	0.175	0.158	70.28	5.32	3.65	0.69	
ReSRGAN-UPos + FT _{IG}	✗	21.14	0.586	0.236	0.182	0.160	72.01	5.35	3.70	0.70	
ReSRGAN-UPos + FT	✗	21.09	0.580	0.235	0.179	0.163	72.69	5.37	3.69	0.71	
ReSRGAN-AMO + FT	✓	21.02	0.581	0.228	0.169	0.161	71.67	5.35	3.68	0.71	

Table 5. **Evaluation on held-out HGGT Test-100.** “FR Low-Lev Dist” refers to full-reference low-level distance metrics; “FR Mid-Lev Dist” and “NR High-Lev. Perceptual Quality” refer to full-reference and no-reference perceptual metrics, respectively. Second column (()) indicates that a method works with *no human GT ranking data* (✓), or requires such GT annotations (✗). “Gold Standard” shows the average of best metric value per quintuplet of test GTs. “OrigsOnly” means no multimodal supervision (no enhanced GT). “Rand” signifies random GT choice (from both enhanced and original), which requires no human annotation, while “UPos” denotes the “positives-only” scenario (uniform sampling from human-ranked positives), the SoTA baseline method from HGGT (marked by *). “FT” refers to fine-tuning (direct optimization); “FT_{HP}” denotes using a higher perceptual loss weight (λ_P), and “FT_{IG}” the inclusion of GAN loss.

5.2. Ablations and Variations

IQA Optimization Refines the Perception-Distortion Trade-off. As noted, our results show a trade-off between mid-level perceptual and NR-IQA metrics, reminiscent of the classic perception-distortion curve [5, 6] (which we also observe, via PSNR and SSIM). We can control this mid-versus-high-level perceptual tradeoff, by simply changing the FT loss weights. For instance, comparing UPos+FT to UPos+FT_{HP} (which increases λ_P), we see that mid-level metrics all improve, while all NR metrics decline.

Discriminators as IQA. One can naturally interpret the discriminator (or critic) of a GAN as a form of NR-IQA model – in fact, it is one specialized to the errors and artifacts of the SR function we are training. However, the FT_{IG} scenario, which keeps the GAN loss during FT, does not greatly impact results (compared to the FT setting); in fact, it largely induces very slight declines. We also tried UPos+FT without an NR-IQA model, instead simply upweighting the GAN loss (treating the critic as an IQA model); however, this results in uniformly worse NR scores, with little change to mid-level metrics (see Supp. §9).

Alternative NR-IQA. While we selected MUSIQ based on our analysis (§3), we also tested FT with an alternative IQA model, PaQ-2-PiQ, based on its high score in Table 2

(see Supp. §9). We find that NIMA, Q-Align, TOPIQ, and (unsurprisingly) MUSIQ all decline, for both SwinIR and ReSRGAN. Nevertheless, it is plausible that a different IQA model (or combination thereof), particularly if fine-tuned for SR, would provide a superior learning signal.

6. Conclusion

As an ill-posed inverse problem, SR struggles with the dichotomy between perceptual quality and reference fidelity. Prior research utilized multiple GTs and human annotations to mitigate this trade-off. In contrast, herein, we focus on improving perceptual quality via neural IQA, enabling us to eschew human annotations. We first analyze existing NR-IQA methods, discerning a candidate for adoption in training, as well as complementary models for evaluation. Then, we devised two ways to apply NR-IQA to SR training: (i) IQA-weighted multimodal GT sampling and (ii) regularized optimization of NR quality. When jointly utilized, our approach outperforms the existing SoTA, which relies on human data, in terms of NR metrics, without sacrificing mid-level reference-based quality scores. We hope it enables future investigation into NR-IQA for SR, the connection between generative modelling and IQA, and SR with domain shift, as IQA does not need paired GT.

References

- [1] Lorenzo Agnolucci, Leonardo Galteri, Marco Bertini, and Alberto Del Bimbo. ARNIQA: Learning distortion manifold for image quality assessment. In *Winter Conference on Applications of Computer Vision (WACV)*, 2024. 3, 5
- [2] Namhyuk Ahn, Byungkon Kang, and Kyung-Ah Sohn. Fast, accurate, and lightweight super-resolution with cascading residual network. In *European Conference on Computer Vision (ECCV)*, 2018. 2
- [3] Yuval Bahat and Tomer Michaeli. Explorable super resolution. In *IEEE Conference on Computer Vision and Pattern Recognition (CVPR)*, 2020. 2
- [4] Simon Baker and Takeo Kanade. Limits on super-resolution and how to break them. *IEEE Transactions on Pattern Analysis and Machine Intelligence (PAMI)*, 2002. 1
- [5] Yochai Blau and Tomer Michaeli. The perception-distortion tradeoff. In *IEEE Conference on Computer Vision and Pattern Recognition (CVPR)*, 2018. 2, 8, 16, 18
- [6] Yochai Blau and Tomer Michaeli. Rethinking lossy compression: The rate-distortion-perception trade-off. In *International Conference on Machine Learning (ICML)*, 2019. 2, 8
- [7] Yochai Blau, Roey Mechrez, Radu Timofte, Tomer Michaeli, and Lihi Zelnik-Manor. The 2018 PIRM challenge on perceptual image super-resolution. In *European Conference on Computer Vision Workshops (ECCVW)*, 2018. 3
- [8] Sebastian Bosse, Dominique Maniry, Klaus-Robert Müller, Thomas Wiegand, and Wojciech Samek. Deep neural networks for no-reference and full-reference image quality assessment. *IEEE Transactions on Image Processing (TIP)*, 2017. 3
- [9] Jianrui Cai, Hui Zeng, Hongwei Yong, Zisheng Cao, and Lei Zhang. Toward real-world single image super-resolution: A new benchmark and a new model. In *International Conference on Computer Vision (ICCV)*, 2019. 16, 18
- [10] Chaofeng Chen and Jiadi Mo. IQA-PyTorch: Pytorch toolbox for image quality assessment. [Online]. Available: <https://github.com/chaofengc/IQA-PyTorch>, 2022. 3
- [11] Chaofeng Chen, Jiadi Mo, Jingwen Hou, Haoning Wu, Liang Liao, Wenxiu Sun, Qiong Yan, and Weisi Lin. TOPIQ: A top-down approach from semantics to distortions for image quality assessment. *IEEE Transactions on Image Processing (TIP)*, 2024. 3, 5, 6, 14
- [12] Du Chen, Jie Liang, Xindong Zhang, Ming Liu, Hui Zeng, and Lei Zhang. Human guided ground-truth generation for realistic image super-resolution. In *IEEE Conference on Computer Vision and Pattern Recognition (CVPR)*, 2023. 2, 3, 4, 6
- [13] Liangyu Chen, Xiaojie Chu, Xiangyu Zhang, and Jian Sun. Simple baselines for image restoration. In *European Conference on Computer Vision (ECCV)*, 2022. 2
- [14] Xiangyu Chen, Xintao Wang, Jiantao Zhou, Yu Qiao, and Chao Dong. Activating more pixels in image super-resolution transformer. In *IEEE Conference on Computer Vision and Pattern Recognition (CVPR)*, 2023. 2
- [15] Zheng Chen, Zongwei Wu, Eduard Zamfir, Kai Zhang, Yulun Zhang, Radu Timofte, Xiaokang Yang, Hongyuan Yu, Cheng Wan, Yuxin Hong, Zhijuan Huang, Yajun Zou, Yuan Huang, Jiamin Lin, Bingnan Han, Xianyu Guan, Yongsheng Yu, Daoan Zhang, Xuanwu Yin, Kunlong Zuo, Jinhua Hao, Kai Zhao, Kun Yuan, Ming Sun, Chao Zhou, Hongyu An, Xinfeng Zhang, Zhiyuan Song, Ziyue Dong, Qing Zhao, Xiaogang Xu, Pengxu Wei, Zhi chao Dou, Guiling Wang, Chih-Chung Hsu, Chia-Ming Lee, Yi-Shiuan Chou, Cansu Korkmaz, A. Murat Tekalp, Yubin Wei, Xiaole Yan, Binren Li, Haonan Chen, Siqi Zhang, Sihan Chen, Amogh Joshi, Nikhil Akalwadi, Sampada Malagi, Palani Yashaswini, Chaitra Desai, Ramesh Ashok Tabib, Ujwala Patil, Uma Mudenagudi, Anjali Sarvaiya, Pooja Choksy, Jagrit Joshi, Shubh Kawa, Kishor Upla, Sushrut Patwardhan, Raghavendra Ramachandra, Sadat Hossain, Geongi Park, S. M. Nadim Uddin, Hao Xu, Yanhui Guo, Aman Urumbekov, Xingzhuo Yan, Wei Hao, Minghan Fu, Isaac Orais, Samuel Smith, Ying Liu, Wangwang Jia, Qisheng Xu, Kele Xu, Weijun Yuan, Zhan Li, Wenqin Kuang, Ruijin Guan, Ruting Deng, Zhao Zhang, Bo Wang, Suiyi Zhao, Yan Luo, Yanyan Wei, Asif Hussain Khan, Christian Micheloni, and Niki Martinel. NTIRE 2024 challenge on image super-resolution ($\times 4$): Methods and results, 2024. 2
- [16] Kevin Clark, Paul Vicol, Kevin Swersky, and David J Fleet. Directly fine-tuning diffusion models on differentiable rewards. *International Conference on Learning Representations (ICLR)*, 2024. 2, 3, 5
- [17] Mauricio Delbracio and Peyman Milanfar. Inversion by direct iteration: An alternative to denoising diffusion for image restoration. *Transactions on Machine Learning Research (TMLR)*, 2023. 2
- [18] Keyan Ding, Kede Ma, Shiqi Wang, and Eero P Simoncelli. Image quality assessment: Unifying structure and texture similarity. *IEEE Transactions on Pattern Analysis and Machine Intelligence (PAMI)*, 2020. 2
- [19] Keyan Ding, Kede Ma, Shiqi Wang, and Eero P Si-

- moncelli. Comparison of full-reference image quality models for optimization of image processing systems. *International Journal of Computer Vision (IJCV)*, 2021. 2, 3
- [20] Keyan Ding, Kede Ma, Shiqi Wang, and Eero P. Simoncelli. Image quality assessment: Unifying structure and texture similarity. *IEEE Transactions on Pattern Analysis and Machine Intelligence (PAMI)*, 2022. 6
- [21] Chao Dong, Chen Change Loy, Kaiming He, and Xiaoou Tang. Learning a deep convolutional network for image super-resolution. In *European Conference on Computer Vision (ECCV)*, 2014. 1, 2
- [22] Chao Dong, Chen Change Loy, and Xiaoou Tang. Accelerating the super-resolution convolutional neural network. In *European Conference on Computer Vision (ECCV)*, 2016. 1, 2
- [23] Ying Fan, Olivia Watkins, Yuqing Du, Hao Liu, Moonkyung Ryu, Craig Boutilier, Pieter Abbeel, Mohammad Ghavamzadeh, Kangwook Lee, and Kimin Lee. DPOK: reinforcement learning for fine-tuning text-to-image diffusion models. In *Neural Information Processing Systems (NeurIPS)*, 2023. 2
- [24] William T Freeman, Thouis R Jones, and Egon C Pasztor. Example-based super-resolution. *IEEE Computer graphics and Applications*, 2002. 1
- [25] Stephanie Fu, Netanel Tamir, Shobhita Sundaram, Lucy Chai, Richard Zhang, Tali Dekel, and Phillip Isola. DreamSim: Learning new dimensions of human visual similarity using synthetic data. *Neural Information Processing Systems (NeurIPS)*, 2023. 19
- [26] Kevin Galim, Wonjun Kang, Yuchen Zeng, Hyung Il Koo, and Kangwook Lee. Parameter-efficient fine-tuning of state space models. *arXiv preprint arXiv:2410.09016*, 2024. 14
- [27] Sara Ghazanfari, Siddharth Garg, Prashanth Krishnamurthy, Farshad Khorrami, and Alexandre Araujo. R-LPIPS: An adversarially robust perceptual similarity metric. *arXiv preprint arXiv:2307.15157*, 2023. 2
- [28] Abhijay Ghildyal and Feng Liu. Shift-tolerant perceptual similarity metric. In *European Conference on Computer Vision (ECCV)*, 2022. 6
- [29] S Alireza Golestaneh, Saba Dadsetan, and Kris M Kitani. No-reference image quality assessment via transformers, relative ranking, and self-consistency. In *Winter Conference on Applications of Computer Vision (WACV)*, 2022. 3
- [30] Ian Goodfellow, Jean Pouget-Abadie, Mehdi Mirza, Bing Xu, David Warde-Farley, Sherjil Ozair, Aaron Courville, and Yoshua Bengio. Generative adversarial nets. *Neural Information Processing Systems (NeurIPS)*, 2014. 2
- [31] Ian J Goodfellow, Jonathon Shlens, and Christian Szegedy. Explaining and harnessing adversarial examples. *International Conference on Learning Representations (ICLR)*, 2015. 5
- [32] Hang Guo, Jinmin Li, Tao Dai, Zhihao Ouyang, Xudong Ren, and Shu-Tao Xia. MambaIR: A simple baseline for image restoration with state-space model. In *European Conference on Computer Vision (ECCV)*, 2024. 2
- [33] Alexander Gushchin, Khaled Abud, Georgii Bychkov, Ekaterina Shumitskaya, Anna Chistyakova, Sergey Lavrushkin, Bader Rasheed, Kirill Malyshев, Dmitriy Vatolin, and Anastasia Antsiferova. Guardians of image quality: Benchmarking defenses against adversarial attacks on image quality metrics. *arXiv preprint arXiv:2408.01541*, 2024. 5
- [34] Martin Heusel, Hubert Ramsauer, Thomas Unterthiner, Bernhard Nessler, and Sepp Hochreiter. GANs trained by a two time-scale update rule converge to a local Nash equilibrium. *Neural Information Processing Systems (NeurIPS)*, 2017. 3
- [35] Vlad Hosu, Hanhe Lin, Tamas Sziranyi, and Dietmar Saupe. KonIQ-10k: An ecologically valid database for deep learning of blind image quality assessment. *IEEE Transactions on Image Processing (TIP)*, 2020. 3, 14
- [36] Edward J Hu, Yelong Shen, Phillip Wallis, Zeyuan Allen-Zhu, Yuanzhi Li, Shean Wang, Lu Wang, and Weizhu Chen. LoRA: Low-rank adaptation of large language models. *International Conference on Learning Representations (ICLR)*, 2022. 5, 14
- [37] Xiaozhong Ji, Yun Cao, Ying Tai, Chengjie Wang, Jilin Li, and Feiyue Huang. Real-world super-resolution via kernel estimation and noise injection. In *IEEE Conference on Computer Vision and Pattern Recognition Workshops (CVPRW)*, 2020. 4
- [38] Younghyun Jo, Seoung Wug Oh, Peter Vajda, and Seon Joo Kim. Tackling the ill-posedness of super-resolution through adaptive target generation. In *IEEE Conference on Computer Vision and Pattern Recognition (CVPR)*, 2021. 2
- [39] Justin Johnson, Alexandre Alahi, and Li Fei-Fei. Perceptual losses for real-time style transfer and super-resolution. In *European Conference on Computer Vision (ECCV)*, 2016. 2
- [40] Bahjat Kawar, Michael Elad, Stefano Ermon, and Jiaming Song. Denoising diffusion restoration models. *Neural Information Processing Systems (NeurIPS)*, 2022. 2
- [41] Junjie Ke, Qifei Wang, Yilin Wang, Peyman Milanfar, and Feng Yang. MUSIQ: Multi-scale image quality transformer. In *International Conference on Computer Vision (ICCV)*, 2021. 2, 3, 5, 6, 14

- [42] Markus Kettunen, Erik Härkönen, and Jaakko Lehtinen. E-LPIPS: robust perceptual image similarity via random transformation ensembles. *arXiv preprint arXiv:1906.03973*, 2019. [2](#)
- [43] Valentin Khrulkov and Artem Babenko. Neural side-by-side: Predicting human preferences for no-reference super-resolution evaluation. In *IEEE Conference on Computer Vision and Pattern Recognition (CVPR)*, 2021. [3](#), [14](#)
- [44] Jiwon Kim, Jung Kwon Lee, and Kyoung Mu Lee. Deeply-recursive convolutional network for image super-resolution. In *IEEE Conference on Computer Vision and Pattern Recognition (CVPR)*, 2016. [2](#)
- [45] Alexey Kurakin, Ian Goodfellow, and Samy Bengio. Adversarial machine learning at scale. *International Conference on Learning Representations (ICLR)*, 2017. [5](#)
- [46] Yongchan Kwon, Eric Wu, Kevin Wu, and James Zou. DataInf: Efficiently estimating data influence in LoRA-tuned LLMs and diffusion models. *International Conference on Learning Representations (ICLR)*, 2024. [14](#)
- [47] Wei-Sheng Lai, Jia-Bin Huang, Narendra Ahuja, and Ming-Hsuan Yang. Deep Laplacian pyramid networks for fast and accurate super-resolution. In *IEEE Conference on Computer Vision and Pattern Recognition (CVPR)*, 2017. [2](#)
- [48] Christian Ledig, Lucas Theis, Ferenc Huszár, Jose Caballero, Andrew Cunningham, Alejandro Acosta, Andrew Aitken, Alykhan Tejani, Johannes Totz, Ze-han Wang, et al. Photo-realistic single image super-resolution using a generative adversarial network. In *IEEE Conference on Computer Vision and Pattern Recognition (CVPR)*, 2017. [2](#)
- [49] Xiaoming Li, Wangmeng Zuo, and Chen Change Loy. Learning generative structure prior for blind text image super-resolution. In *IEEE Conference on Computer Vision and Pattern Recognition (CVPR)*, 2023. [19](#)
- [50] Jingyun Liang, Jiezhang Cao, Guolei Sun, Kai Zhang, Luc Van Gool, and Radu Timofte. SwinIR: Image restoration using swin transformer. In *International Conference on Computer Vision (ICCV)*, 2021. [2](#), [6](#), [14](#)
- [51] Jie Liang, Hui Zeng, and Lei Zhang. Details or artifacts: A locally discriminative learning approach to realistic image super-resolution. In *IEEE Conference on Computer Vision and Pattern Recognition (CVPR)*, 2022. [2](#)
- [52] Youwei Liang, Junfeng He, Gang Li, Peizhao Li, Arseniy Klimovskiy, Nicholas Carolan, Jiao Sun, Jordi Pont-Tuset, Sarah Young, Feng Yang, et al. Rich human feedback for text-to-image generation. In *IEEE Conference on Computer Vision and Pattern Recognition (CVPR)*, 2024. [3](#)
- [53] Liting Lin, Heng Fan, Zhipeng Zhang, Yaowei Wang, Yong Xu, and Haibin Ling. Tracking meets LoRA: Faster training, larger model, stronger performance. In *European Conference on Computer Vision (ECCV)*, 2024. [14](#)
- [54] Yue Liu, Yunjie Tian, Yuzhong Zhao, Hongtian Yu, Lingxi Xie, Yaowei Wang, Qixiang Ye, Jianbin Jiao, and Yunfan Liu. VMamba: Visual state space model. In *Neural Information Processing Systems (NeurIPS)*, 2024. [2](#)
- [55] Yujia Liu, Chenxi Yang, Dingquan Li, Jianhao Ding, and Tingting Jiang. Defense against adversarial attacks on no-reference image quality models with gradient norm regularization. In *IEEE Conference on Computer Vision and Pattern Recognition (CVPR)*, 2024. [5](#)
- [56] Andreas Lugmayr, Martin Danelljan, Luc Van Gool, and Radu Timofte. SRFFlow: Learning the super-resolution space with normalizing flow. In *European Conference on Computer Vision (ECCV)*, 2020. [2](#)
- [57] Chao Ma, Chih-Yuan Yang, Xiaokang Yang, and Ming-Hsuan Yang. Learning a no-reference quality metric for single-image super-resolution. *Computer Vision and Image Understanding (CVIU)*, 2017. [3](#)
- [58] Cheng Ma, Yongming Rao, Yean Cheng, Ce Chen, Jiwen Lu, and Jie Zhou. Structure-preserving super resolution with gradient guidance. In *IEEE Conference on Computer Vision and Pattern Recognition (CVPR)*, 2020. [2](#)
- [59] Anish Mittal, Anush Krishna Moorthy, and Alan Conrad Bovik. No-reference image quality assessment in the spatial domain. *IEEE Transactions on Image Processing (TIP)*, 2012. [3](#), [14](#)
- [60] Jim Nilsson and Tomas Akenine-Möller. Understanding SSIM. *arXiv preprint arXiv:2006.13846*, 2020. [18](#)
- [61] Xingang Pan, Xiaohang Zhan, Bo Dai, Dahua Lin, Chen Change Loy, and Ping Luo. Exploiting deep generative prior for versatile image restoration and manipulation. *IEEE Transactions on Pattern Analysis and Machine Intelligence (PAMI)*, 2021. [2](#)
- [62] JoonKyu Park, Sanghyun Son, and Kyoung Mu Lee. Content-aware local GAN for photo-realistic super-resolution. In *International Conference on Computer Vision (ICCV)*, 2023. [2](#)
- [63] Seung Ho Park, Young Su Moon, and Nam Ik Cho. Perception-oriented single image super-resolution using optimal objective estimation. In *IEEE Conference on Computer Vision and Pattern Recognition (CVPR)*, 2023. [2](#)

- [64] Jonathan W Peirce. Understanding mid-level representations in visual processing. *Journal of Vision (JOV)*, 2015. 19
- [65] Zygmunt Pizlo. Perception viewed as an inverse problem. *Vision research*, 41(24):3145–3161, 2001. 1
- [66] Nikolay Ponomarenko, Oleg Ieremeiev, Vladimir Lukin, Karen Egiazarian, Lina Jin, Jaakko Astola, Benoit Vozel, Kacem Chehdi, Marco Carli, Federica Battisti, et al. Color image database TID2013: Peculiarities and preliminary results. In *European workshop on visual information processing (EUVIP)*. IEEE, 2013. 3
- [67] Mihir Prabhudesai, Anirudh Goyal, Deepak Pathak, and Katerina Fragkiadaki. Aligning text-to-image diffusion models with reward backpropagation. *arXiv preprint arXiv:2310.03739*, 2023. 2
- [68] Michele A Saad, Alan C Bovik, and Christophe Charrier. A DCT statistics-based blind image quality index. *IEEE Signal Processing Letters*, 2010. 2, 3
- [69] Chitwan Saharia, Jonathan Ho, William Chan, Tim Salimans, David J Fleet, and Mohammad Norouzi. Image super-resolution via iterative refinement. *IEEE Transactions on Pattern Analysis and Machine Intelligence (PAMI)*, 2022. 2
- [70] Divya Saxena and Jianlong Cao. Generative adversarial networks (GANs) challenges, solutions, and future directions. *ACM Computing Surveys (CSUR)*, 2021. 2
- [71] Wenzhe Shi, Jose Caballero, Ferenc Huszár, Johannes Totz, Andrew P Aitken, Rob Bishop, Daniel Rueckert, and Zehan Wang. Real-time single image and video super-resolution using an efficient sub-pixel convolutional neural network. In *IEEE Conference on Computer Vision and Pattern Recognition (CVPR)*, 2016. 2
- [72] Shaolin Su, Qingsen Yan, Yu Zhu, Cheng Zhang, Xin Ge, Jinqiu Sun, and Yanning Zhang. Blindly assess image quality in the wild guided by a self-adaptive hyper network. In *IEEE Conference on Computer Vision and Pattern Recognition (CVPR)*, 2020. 3
- [73] Christian Szegedy, Wojciech Zaremba, Ilya Sutskever, Joan Bruna, Dumitru Erhan, Ian Goodfellow, and Rob Fergus. Intriguing properties of neural networks. In *International Conference on Learning Representations (ICLR)*, 2014. 5
- [74] Hossein Talebi and Peyman Milanfar. NIMA: Neural image assessment. *IEEE Transactions on Image Processing (TIP)*, 2018. 2, 3, 5, 6
- [75] Huixuan Tang, Neel Joshi, and Ashish Kapoor. Learning a blind measure of perceptual image quality. In *IEEE Conference on Computer Vision and Pattern Recognition (CVPR)*, 2011. 2, 3
- [76] Radu Timofte, Vincent De Smet, and Luc Van Gool. Anchored neighborhood regression for fast example-based super-resolution. In *International Conference on Computer Vision (ICCV)*, 2013. 2
- [77] Radu Timofte, Vincent De Smet, and Luc Van Gool. A+: Adjusted anchored neighborhood regression for fast super-resolution. In *Proceedings of the Asian Conference on Computer Vision (ACCV)*, 2015. 2
- [78] Ilya Tolstikhin, Olivier Bousquet, Sylvain Gelly, and Bernhard Schoelkopf. Wasserstein auto-encoders. *arXiv preprint arXiv:1711.01558v3*, 2018. 19
- [79] Rao Muhammad Umer and Christian Micheloni. Deep cyclic generative adversarial residual convolutional networks for real image super-resolution. In *European Conference on Computer Vision Workshops (ECCVW)*, 2020. 2
- [80] International Telecommunication Union. Methodology for the subjective assessment of the quality of television pictures. *Recommendation ITU-R BT.500-13*, 2012. Geneva, Switzerland. 18
- [81] Narasimhan Venkatanath, D Praneeth, Maruthi Chandrasekhar Bh, Sumohana S Channappayya, and Swarup S Medasani. Blind image quality evaluation using perception based features. In *2015 Twenty first national conference on communications (NCC)*. IEEE, 2015. 3
- [82] Jianyi Wang, Kelvin CK Chan, and Chen Change Loy. Exploring CLIP for assessing the look and feel of images. In *Proceedings of the National Conference on Artificial Intelligence (AAAI)*, 2023. 3
- [83] Jianyi Wang, Zongsheng Yue, Shangchen Zhou, Kelvin CK Chan, and Chen Change Loy. Exploiting diffusion prior for real-world image super-resolution. *International Journal of Computer Vision (IJCV)*, 2024. 2
- [84] Xintao Wang, Ke Yu, Shixiang Wu, Jinjin Gu, Yihao Liu, Chao Dong, Yu Qiao, and Chen Change Loy. ESRGAN: Enhanced super-resolution generative adversarial networks. In *European Conference on Computer Vision Workshops (ECCVW)*, 2018. 2, 6, 14
- [85] Xintao Wang, Liangbin Xie, Chao Dong, and Ying Shan. Real-ESRGAN: Training real-world blind super-resolution with pure synthetic data. In *International Conference on Computer Vision (ICCV)*, 2021. 4, 6, 14
- [86] Zhou Wang, Alan C Bovik, Hamid R Sheikh, and Eero P Simoncelli. Image quality assessment: from error visibility to structural similarity. *IEEE Transactions on Image Processing (TIP)*, 2004. 2, 6
- [87] Haoning Wu, Erli Zhang, Liang Liao, Chaofeng Chen, Jingwen Hou, Annan Wang, Wenxiu Sun, Qiong Yan, and Weisi Lin. Exploring video quality assessment on user generated contents from aesthetic

- and technical perspectives. In *International Conference on Computer Vision (ICCV)*, 2023. 18
- [88] Haoning Wu, Zicheng Zhang, Weixia Zhang, Chaofeng Chen, Liang Liao, Chunyi Li, Yixuan Gao, Annan Wang, Erli Zhang, Wenxiu Sun, Qiong Yan, Xiongkuo Min, Guangtao Zhai, and Weisi Lin. Q-Align: Teaching LMMs for visual scoring via discrete text-defined levels. In *International Conference on Machine Learning (ICML)*, 2024. 3, 5, 6, 14
- [89] Rongyuan Wu, Lingchen Sun, Zhiyuan Ma, and Lei Zhang. One-step effective diffusion network for real-world image super-resolution. *Neural Information Processing Systems (NeurIPS)*, 2024. 2, 18
- [90] Rongyuan Wu, Tao Yang, Lingchen Sun, Zhengqiang Zhang, Shuai Li, and Lei Zhang. SeeSR: Towards semantics-aware real-world image super-resolution. In *IEEE Conference on Computer Vision and Pattern Recognition (CVPR)*, 2024. 18
- [91] Bin Xia, Yulun Zhang, Shiyin Wang, Yitong Wang, Xinglong Wu, Yapeng Tian, Wenming Yang, and Luc Van Gool. DiffIR: Efficient diffusion model for image restoration. In *International Conference on Computer Vision (ICCV)*, 2023. 2
- [92] Jiazheng Xu, Xiao Liu, Yuchen Wu, Yuxuan Tong, Qinkai Li, Ming Ding, Jie Tang, and Yuxiao Dong. ImageReward: Learning and evaluating human preferences for text-to-image generation. *Neural Information Processing Systems (NeurIPS)*, 2024. 2, 3
- [93] Jianchao Yang, Zhaowen Wang, Zhe Lin, Scott Cohen, and Thomas Huang. Coupled dictionary training for image super-resolution. *IEEE Transactions on Image Processing (TIP)*, 2012. 2
- [94] Sidi Yang, Tianhe Wu, Shuwei Shi, Shanshan Lao, Yuan Gong, Mingdeng Cao, Jiahao Wang, and Yujiu Yang. MANIQA: Multi-dimension attention network for no-reference image quality assessment. In *IEEE Conference on Computer Vision and Pattern Recognition (CVPR)*, 2022. 3
- [95] Tao Yang, Rongyuan Wu, Peiran Ren, Xuansong Xie, and Lei Zhang. Pixel-aware stable diffusion for realistic image super-resolution and personalized stylization. In *European Conference on Computer Vision (ECCV)*, 2024. 2, 18
- [96] Jie-En Yao, Li-Yuan Tsao, Yi-Chen Lo, Roy Tseng, Chia-Che Chang, and Chun-Yi Lee. Local implicit normalizing flow for arbitrary-scale image super-resolution. In *IEEE Conference on Computer Vision and Pattern Recognition (CVPR)*, 2023. 2
- [97] Zhenqiang Ying, Haoran Niu, Praful Gupta, Dhruv Mahajan, Deepti Ghadiyaram, and Alan Bovik. From patches to pictures (PaQ-2-PiQ): Mapping the perceptual space of picture quality. In *IEEE Conference on Computer Vision and Pattern Recognition (CVPR)*, 2020. 3, 5, 14
- [98] Lin Zhang, Lei Zhang, and Alan C Bovik. A feature-enriched completely blind image quality evaluator. *IEEE Transactions on Image Processing (TIP)*, 2015. 3, 14
- [99] Richard Zhang, Phillip Isola, Alexei A Efros, Eli Shechtman, and Oliver Wang. The unreasonable effectiveness of deep features as a perceptual metric. In *IEEE Conference on Computer Vision and Pattern Recognition (CVPR)*, 2018. 2
- [100] Weixia Zhang, Kede Ma, Jia Yan, Dexiang Deng, and Zhou Wang. Blind image quality assessment using a deep bilinear convolutional neural network. *IEEE Transactions on Circuits and Systems for Video Technology*, 2020. 3
- [101] Weixia Zhang, Guangtao Zhai, Ying Wei, Xiaokang Yang, and Kede Ma. Blind image quality assessment via vision-language correspondence: A multitask learning perspective. In *IEEE Conference on Computer Vision and Pattern Recognition (CVPR)*, 2023. 3, 5
- [102] Yulun Zhang, Kunpeng Li, Kai Li, Lichen Wang, Bin-neng Zhong, and Yun Fu. Image super-resolution using very deep residual channel attention networks. In *European Conference on Computer Vision (ECCV)*, 2018. 2, 6
- [103] Yuzhe Zhang, Jiawei Zhang, Hao Li, Zhouxia Wang, Luwei Hou, Dongqing Zou, and Liheng Bian. Diffusion-based blind text image super-resolution. In *IEEE Conference on Computer Vision and Pattern Recognition (CVPR)*, 2024. 19
- [104] Heliang Zheng, Huan Yang, Jianlong Fu, Zheng-Jun Zha, and Jiebo Luo. Learning conditional knowledge distillation for degraded-reference image quality assessment. In *International Conference on Computer Vision (ICCV)*, 2021. 3

Augmenting Perceptual Super-Resolution via Image Quality Predictors

Supplementary Material

7. Complete Analysis of NR-IQA metrics

In §3.1 of the main paper, we present accuracy of only top 7 NR-IQA metrics on the subset of SBS180K [43] train set. Here, in Table 6, we present accuracy of 20 NR-IQA metrics and their variants (42 in total) on the same subset. We make two main observations. First, unsurprisingly, recent NR-IQA metrics (e.g. PaQ-2-PiQ [97], MUSIQ [41], Q-Align [88]) are more aligned with human preferences than the classical ones (e.g. NIQE [98] and BRISQUE [59]), calling for wider adaptation of more recent metrics in evaluating SR models. Second, the IQA dataset on which the metric is trained affects its accuracy in determining human preference for SR. For instance, TOPIQ [11] trained using KonIQ [35] dataset is more aligned with human judgement (73.06%) than the one trained using FLIVE [97] dataset (58.19%). Results indicate an opportunity to create a no-reference IQA dataset exclusively for training NR metrics for SR.

7.1. Remark on NR-IQA Choices

As discussed in §3, our choice of MUSIQ for weighted sampling and fine-tuning comes from several considerations. First, on SBS-180K, MUSIQ is highly performant (see Phase II analysis of §3.1). Second, on HGGT (§3.2), MUSIQ has the best positive misalignment, meaning it is the least likely to misrank a positive. It is also relatively efficient for both inference and back-propagation.

In our application, distinguishing between the quality of positives would seem to be more significant, since we are ideally training the SR model in a manner that focuses on the highest quality images (i.e., incorrect ordering of the lower-ranked images will not affect our method; hence, fine-grained differentiation between the high-ranked images is more important). Nevertheless, it is true that MUSIQ (like all NR-IQA models evaluated here) does not perform well on negative misalignment. However, we do not expect this to have a large impact on training, due to the *rarity* of negatives. Specifically, in HGGT-train, only $\sim 6\%$ of tuples contain negatives and, among those, MUSIQ ranks a negative the highest in $\sim 34\%$ of cases. Thus, our AMO model will be exposed to a negative in only $\sim 2\%$ of examples. Hence, merely for numerical magnitude, discernment for positives is likely to be more impactful than for negatives. Of course, this reasoning is somewhat specific to the HGGT setup.

Further, in terms of evaluation, note that we choose NIMA and Q-Align specifically because they perform best on the SBS-180K samples on which MUSIQ fails. Ideally,

this complementarity would help ensure that errors induced by shortcomings of MUSIQ could potentially be detected by the other NR-IQA metrics. Nevertheless, as seen in Table 7, our experiments with PaQ-2-PiQ (which was among the best models according to Table 2) show MUSIQ outperforms it.

Regardless, our method does not specifically require the use of MUSIQ. Indeed, we believe further advancements in NR-IQA models (e.g., approaches specific to SR image quality, adversarially robust models) will be applicable to our method as well.

8. Methodological Details

8.1. Sampling Details

The altered sampling (§4.2) is trained identically to the standard HGGT version, just replacing the uniform nature of the GT sampling. The only additional parameter is the temperature, τ , which we set to 10 for both SMA and SMP.

8.2. Hardware and Timing

Similar to HGGT, we train on four A100 GPUs for 300K iterations. This takes ~ 23 and ~ 32 hours for SwinIR and RealESRGAN, respectively, with an additional ~ 3.5 hours for fine-tuning.

8.3. Fine-Tuning Details

Unless otherwise noted, we use the same training parameters as HGGT. We fine-tune for only 20,000 steps and set $\lambda_Q = 0.05$ as the FT MUSIQ weight. For SwinIR and RealESRGAN, respectively, we change the learning rate to 5×10^{-6} (halved at 5K steps) and 5×10^{-5} . Recall that, by default, the adversarial loss is not used (i.e., $\lambda_A = 0$) during FT (but see §9). Architecturally, LoRA weights are inserted slightly differently: on SwinIR [50], only the multilayer perceptions are altered (rank 48), while on the convolutional RealESRGAN [84, 85], only the layers in the Residual-in-Residual Dense Blocks (RRDBs) are altered (rank 24). This follows other works, including the original LoRA paper [36], which only apply LoRA-based fine-tuning to a subset of layers (e.g., see [26, 46, 53]). Recall that LoRA cannot increase the capacity (i.e., expressive capability) of the networks (as the new weights can simply be merged into the old ones at inference time, which also prevents any run-time penalty to inference), so comparisons to non-FT models are fair. Fine-tuning is run for 20K steps, as opposed to the 300K in stage two training. Brief exploration of hyper-parameters (beyond those considered in §5)

Method	Acc (%)	Method	Acc (%)	Method	Acc (%)	Method	Acc (%)	Method	Acc (%)
paq2piq	76.41	arniqa-kadid	71.48	tres	69.98	arniqa-clive	66.81	brisque_matlab	61.00
nima	74.91	arniqa-flive	71.30	clipiqqa+_vitL14_512	69.98	arniqa-spaq	66.73	wadiqam_nr	60.30
musiq	74.47	topiq_nr-spaq	71.30	musiq-paq2piq	69.98	arniqa	66.46	topiq_nr-flive	58.19
liqe	74.03	arniqa-csiq	71.21	maniqa-pipal	69.63	musiq-ava	66.37	ilniqe	57.92
arniqa-tid	74.03	musiq-spaq	70.86	clipiqqa+_rn50_512	69.10	nrqm	65.05	niqe	56.43
qalign	73.77	nima-vgg16-ava	70.77	dbcnn	68.49	cnniqa	63.73	brisque	55.11
topiq_nr	73.06	maniqa	70.51	clipiqqa	68.40	tres-flive	63.29	niqe_matlab	51.94
hyperiqa	72.27	clipiqqa+	70.25	arniqa-live	68.05	pi	62.41	piqe	46.21
liqe_mix	71.48	maniqa-kadid	70.16						

Table 6. **Phase I analysis on SBS180K dataset.** Accuracy of 20 NR-IQA metrics and their variants on the subset (1212 image pairs) of train set of SBS180K dataset. We denote a metric by its ‘Model Name’ as defined in IQA-PyTorch toolbox (<https://iqa-pytorch.readthedocs.io/en/latest/ModelCard.html>). We use the default configuration for all metrics and their variants.

Model	NR	λ_A	∅	FR Low-Lev. Dist.			FR Mid-Lev. Dist.			NR High-Lev. Perceptual Quality		
				PSNR ↑	SSIM ↑	LPIPS ↓	LPIPS-ST ↓	DISTS ↓	MUSIQ ↑	NIMA ↑	Q-Align ↑	TOPIQ ↑
Gold Standard	—	—	✗	—	—	—	—	—	69.64	5.28	3.78	0.69
SwinIR-UPos*	—	—	✗	22.30	0.647	0.169	0.129	0.123	66.39	5.16	3.56	0.62
SwinIR-UPos + FT _{HP}	M	0	✗	22.17	0.642	0.166	0.123	0.122	68.38	5.23	3.64	0.65
SwinIR-UPos + FT _{IG}	M	0.1	✗	22.03	0.635	0.168	0.122	0.123	69.37	5.24	3.69	0.66
SwinIR-UPos + FT _{NNR,IG×2}	—	0.2	✗	22.25	0.646	0.171	0.130	0.124	66.61	5.16	3.56	0.61
SwinIR-UPos + FT _{NNR,IG×5}	—	0.5	✗	22.20	0.644	0.174	0.134	0.125	66.61	5.16	3.56	0.61
SwinIR-UPos + FT _{PaQ2PiQ}	P	0	✗	22.29	0.649	0.166	0.120	0.121	67.29	5.18	3.58	0.62
SwinIR-UPos + FT	M	0	✗	22.01	0.633	0.169	0.123	0.124	69.70	5.26	3.70	0.67
SwinIR-AMO + FT	M	0	✓	21.77	0.624	0.174	0.121	0.128	70.81	5.29	3.75	0.70
RESRGAN-UPos*	—	—	✗	21.54	0.608	0.233	0.192	0.158	65.93	5.25	3.47	0.63
RESRGAN-UPos + FT _{HP}	M	0	✗	21.30	0.595	0.226	0.175	0.158	70.28	5.32	3.65	0.69
RESRGAN-UPos + FT _{IG}	M	0.1	✗	21.14	0.586	0.236	0.182	0.160	72.01	5.35	3.70	0.70
RESRGAN-UPos + FT _{NNR,IG×2}	—	0.2	✗	21.35	0.600	0.234	0.191	0.157	65.94	5.22	3.45	0.63
RESRGAN-UPos + FT _{NNR,IG×5}	—	0.5	✗	21.25	0.598	0.237	0.195	0.158	65.78	5.22	3.46	0.63
RESRGAN-UPos + FT _{PaQ2PiQ}	P	0	✗	21.46	0.605	0.228	0.182	0.157	67.26	5.22	3.51	0.64
RESRGAN-UPos + FT	M	0	✗	21.09	0.580	0.235	0.179	0.163	72.69	5.37	3.69	0.71
RESRGAN-AMO + FT	M	0	✓	21.02	0.581	0.228	0.169	0.161	71.67	5.35	3.68	0.71

Table 7. **Additional evaluation on held-out HGGT Test-100.** As in Table 5 in the main paper, “FR Low-Lev Dist” refers to full-reference low-level distance metrics; “FR Mid-Lev Dist” and “NR High-Lev. Perceptual Quality” refer to full-reference and no-reference perceptual metrics, respectively. Second column (∅) indicates that a method works with *no human GT ranking data* (✓), or requires such GT annotations (✗). “Gold Standard” shows the average of best metric value per quintuplet of test GTs. “UPos” denotes the “positives-only” scenario (uniform sampling from human-ranked positives), the SoTA baseline method from HGGT (marked by *). “FT” refers to fine-tuning (direct optimization): “FT_{IG}” includes the adversarial loss during FT, “FT_{NNR,IG×2}” and “FT_{NNR,IG×5}” have no NR term during FT, but increase the GAN loss (two and five times, respectively), and finally “FT_{PaQ2PiQ}” replaces MUSIQ with PaQ-2-PiQ. The NR column denotes which NR-IQA model is used (M: MUSIQ, P: PaQ-2-PiQ, -: None), while λ_A is the adversarial loss weight (the standard HGGT default for training is 0.1). We also show our best method: AMO+FT, which combines IQA-based sampling with our standard FT settings, for comparison. Note that AMO+FT is the only method here that *does not use human annotations*. We remark also that the NR-IQA models have the following ranges: MUSIQ (0-100), NIMA (0-10), Q-Align (1,5), and TOPIQ (0-1).

yielded minimal changes, likely due to rapid convergence of the low-rank (i.e., low capacity) weights ϕ .

9. Detailed Results on Ablations and Variations

In this section, we consider additional FT variations: (i) using a GAN discriminator instead of an NR-IQA model (using two different loss weights) and (ii) replacing Q (set as MUSIQ) with a different NR-IQA model (PaQ-2-PiQ). The point of (i) is to check whether the GAN critic, which is effectively an NR-IQA model that has been specialized to the SR model in question, can be used for fine-tuning, instead

of a separate NR-IQA model. For (ii), we wish to check if our choice of optimized NR metric, MUSIQ, is reasonable.

Our results on these variations are in Table 7. Since FT optimizes MUSIQ, we focus on the other NR metrics, especially Q-Align and NIMA (since they perform the best on examples where MUSIQ fails; see §3.1). First, we find that including the GAN loss in the standard scenario has a slight negative effect on the NR metrics; however, removing the NR metric term and strengthening the adversarial term (i.e., “FT_{NNR,IG×2}” and “FT_{NNR,IG×5}”) has a significantly more negative impact on the NR evaluations. This suggests that



Figure 5. Structured Noise due to naive NR-IQA optimization. The left three insets show an image and two close-ups that was fine-tuned *without* LoRA, whereas the right three show the effect of using LoRA. Note the patterns that form in the sky and the strangely coloured pixels that appear around certain edges (e.g., the blue/red grid in the second inset) when LoRA is not used.

the critic network *cannot* replace the NR-IQA model, even though it is intuitively similar to one (in that it evaluates the image quality of a single input, which can be used as a learning signal). We conjecture this is because the critic is trained to detect the idiosyncrasies of its associated generator (at a specific point in time), rather than match human quality estimates; hence, optimizing it more aggressively may reduce those specific issues that the critic has detected, but not necessarily increase general quality.

Second, we tried to replace MUSIQ with PaQ-to-PiQ. We find that this tends to improve low and mid level distortion (though the relation is less clear for RealESRGAN, especially with LPIPS-ST), but worsens NIMA and Q-Align. We therefore choose to stay with MUSIQ for our main results. In general, we do not wish to claim that MUSIQ is an optimal starting point for FT; however, it does suggest our analysis is a useful approach to initially identifying a good NR-IQA network. Nevertheless, we suspect that using an alternative NR-IQA model (with sufficient hyper-parameter exploration), fine-tuning a new model, combining multiple models, or training a model specific to SR could all be potentially useful future approaches to improving results.

10. Additional Qualitative Examples

10.1. Additional Comparative Samples

Additional comparisons are shown in Fig. 6 (as in Fig. 4). Our method (AMO or AMO+FT) is universally sharper and more detailed than UPos (e.g., see the hair in row three). Further, it can occasionally remove some of the noise present in the UPos scenario (see the tongue of the red panda). Importantly, our approach may not generate details that are identical to the GT, but it does construct sharp image content without jarring unrealistic artifacts (e.g., see rows one and four; the plants, rocks, and bricks have slightly different details, but they are plausible and of similar aesthetic quality nonetheless).

10.2. Additional Naive Optimization Visualizations

In Fig. 5, as in Fig. 3, we show the subtle “grid-like” artifacts that appear when naive NR-IQA optimization is per-

formed. In particular, we see spatial patterns form in homogeneous areas (e.g., stripes in the sky or on the tan coloured island), while other areas exhibit highly unnatural colours (e.g., the alternating blue-red pixels on the dark rock). These small, pixel-scale artifacts are akin to an adversarial attack on MUSIQ; hence, much of this structured noise is alleviated by applying LoRA (right insets). Other methods of handling such artifacts, such as an adversarially robust NR-IQA model, may also be effective, but we leave this to future work.

11. Additional Results on RealSR

We provide results on the RealSRv3 [9] dataset in Table 8. Similar to the HGGT test dataset, we find that *our method is superior in terms of every NR-IQA metric*, at the expense of the exact pixel-level details measured by PSNR and SSIM (following the perception-distortion tradeoff [5]). However, according to mid-level FR metrics, our method *also* performs well, obtaining the best scores on LPIPS-ST, and even on LPIPS and DISTs for SwinIR. This suggests our method can improve image quality, while maintaining the most salient perceptual details (e.g., mid-level textures) of the underlying GT.

12. Comparative Evaluation via User Study

Similar to the HGGT user study, we invite 12 volunteers to evaluate their preference between SwinIR-AMO+FT and SwinIR-UPos, using the HGGT Test-100 dataset. Each volunteer evaluates 25 image pairs (25% of the dataset), with each image in Test-100 being seen an equal number of times (namely, three). For each pair (SwinIR-AMO+FT vs. SwinIR-UPos), we employ an image comparison slider. This tool places two images on top of each other, and allows volunteers to use a slider to alternate between them (see Fig. 7 for a visualization). The order of presentation of the two methods (left vs. right) is randomized to eliminate bias. For each individual, we obtain a single score, which is the percentage of the time that they prefer our method (across those 25 images). The average score across raters is **69.7%** (median: 68.0%; empirical standard error of the

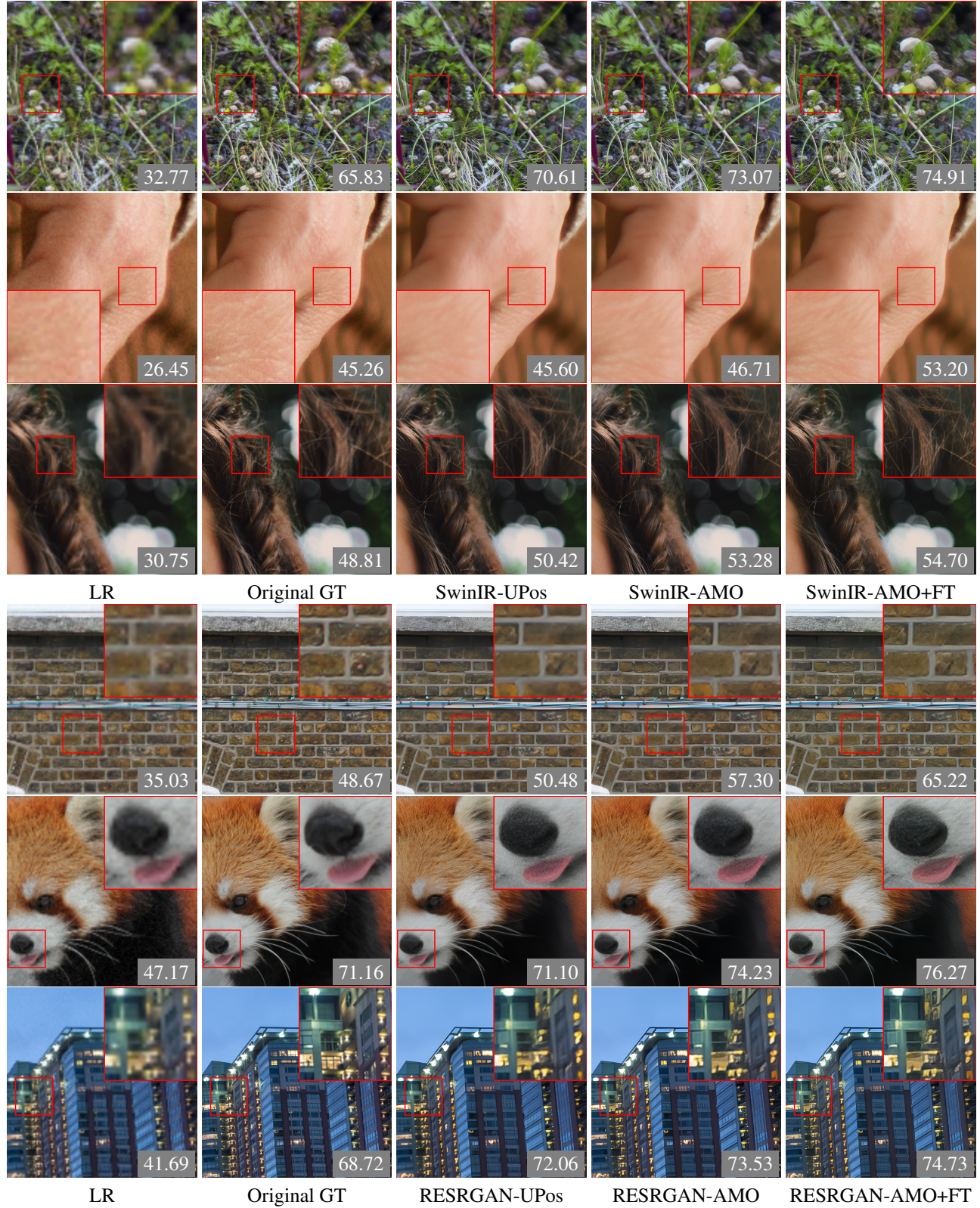


Figure 6. Qualitative results with NR-IQA guidance. Following the notation of Table 5, columns 3-5 are (top 3 rows) SwinIR-UPos, SwinIR-AMO, and SwinIR-AMO + FT, and (bottom 3 rows) Real-ESRGAN-UPos, Real-ESRGAN-AMO, and Real-ESRGAN-AMO + FT. We show MUSIQ scores in insets. Qualitatively, we see improved performance as we move across the ‘UPos’, ‘AMO’, and ‘AMO-FT’ methods, particularly in terms of sharpness and detail generation. Zoom in for details.

Model	FR PSNR ↑ SSIM ↑ LPIPS ↓	FR Low-Lev. Dist.			FR Mid-Lev. Dist.			NR High-Lev. Perceptual Quality		
		FR PSNR ↑	FR SSIM ↑	FR LPIPS ↓	FR LPIPS-ST ↓	FR DISTST ↓	NR MUSIQ ↑	NR NIMA ↑	NR Q-Align ↑	NR TOPIQ ↑
SwinIR-OrigOnly	✓	26.05	0.746	0.37	0.38	0.20	31.37	4.24	2.88	0.23
SwinIR-UPos*	✗	26.02	0.747	0.35	0.37	0.20	33.69	4.31	2.95	0.24
SwinIR-AMO	✓	25.99	0.747	0.34	0.37	0.19	34.86	4.32	2.96	0.25
SwinIR-AMO + FT	✓	25.96	0.742	0.33	0.35	0.19	39.25	4.37	2.99	0.30
RESRGAN-OrigOnly	✓	25.90	0.758	0.27	0.27	0.16	46.11	4.80	3.40	0.32
RESRGAN-UPos*	✗	25.45	0.750	0.28	0.26	0.17	52.74	4.95	3.53	0.41
RESRGAN-AMO	✓	25.22	0.745	0.28	0.25	0.17	54.73	4.97	3.57	0.45
RESRGAN-AMO + FT	✓	24.71	0.718	0.32	0.24	0.19	65.12	5.03	3.77	0.63

Table 8. **Additional evaluation on the RealSRv3 [9].** Following Table 7, we evaluate the four main models on the RealSR V3 dataset, which consists of 100 test images captured using two DSLR cameras (Canon 5D3 and Nikon D810). Our methods (“AMO” and “AMO + FT”) achieve the highest no-reference perceptual metric (i.e., NR-IQA) scores, outperforming both “OrigsOnly” (without enhanced GT) and “UPos” (the SOTA baseline from HGGT, marked by *).

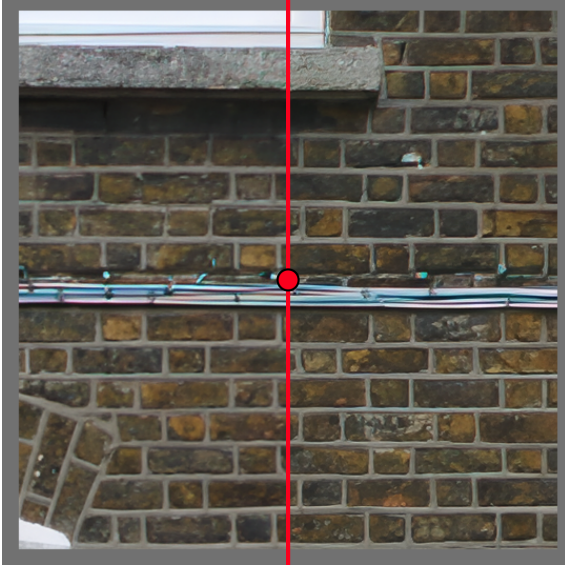


Figure 7. **User study example.** Users can move the slider to alternate between 2 images.

mean: 4.8%), suggesting our algorithm is preferred over the HGGT-based UPos approach at a more than 2:1 ratio, *despite their use of human annotations*, which ours does not use. Following similar image quality assessment protocols (e.g., [80]), a simple single-sample one-sided t-test finds the rater mean significantly above 50% ($p < 0.01$; 95% confidence interval: [60.2%, 79.1%]).

13. Remark on Evaluation Metric Types and Nomenclature

The perception-distortion tradeoff [5] necessitates a complex suite of evaluation metrics that consider different aspects of the SR outputs, including pixel-level fidelity to a GT image and standalone image quality. Some works (e.g., [90]) even utilize performance on downstream vision tasks

(e.g., detection or segmentation) as a form of checking semantic preservation. In this work, we therefore also include a continuum of metrics, which we hope will cover various points along the perception-distortion frontier. These metrics are often categorized along two different axes: (i) the use of a reference and (ii) the level of visual abstraction (low vs mid vs high).

NR vs FR. The first form of metric categorization is full-reference (FR) vs no-reference (NR). In general, FR metrics (which have access to a GT) measure distortion, while NR metrics (which do not use a GT) measure perceptual quality. For NR metrics, there is no way to measure distortion; however, there are many different aspects of perceptual quality that can be considered, ranging from simple sharpness to differentiating aesthetic vs technical quality (e.g., [87]). Hence, it is common (e.g., [89, 90, 95]) to use a set of NR-IQA models, which presumably complement each other, as we do (see §3 and §7.1 for the discussion behind our metric choices). For FR metrics, there is more of a spectrum (i.e., they can include some aspects of perceptual information, in addition to measuring distortion). PSNR and other per-pixel distances have no notion of perception, operating directly on pixel values. SSIM is meant to be more perceptual, but is a simple, hand-crafted similarity operating on colours, limiting its perceptual modelling capabilities [60]. In contrast, LPIPS and DISTST utilize neural network features, aiming to capture certain aspects of human vision. They are therefore *more perceptual* than, e.g., PSNR, as they will tolerate some pixel differences (distortion) if they improve network activation similarity. Even further along this curve towards greater perceptual sensitivity is LPIPS-ST, a model designed specifically to ignore small spatial shifts (which are devastating to pixel-level distortion measures). Indeed, in many cases, we find that LPIPS-ST actually agrees with the NR-IQA perceptual metrics more closely than LPIPS or DISTST, despite being an FR metric. Hence, FR metrics can occupy a range across the perception-distortion curve.

Abstraction Level. A separate nomenclature arises based on the *type of information* that impacts the model. It is based on the hierarchical nature of *biological* vision (e.g., [64]), but is also commonly used throughout computer vision (e.g., [25]). Specifically, we divide visual processes into *low-level*, relating to raw colours and 2D geometry (e.g., edges); *mid-level*, encompassing “groupings” of more basic features into patterns and textures, as well as local 3D structures; and *high-level*, pertaining to semantics (e.g., scene classification) and representational abstraction (e.g., holistic interpretations of the image). For this reason, we refer to PSNR and SSIM, which operate directly on colours, as low-level, while LPIPS and DISTS are mid-level, as they respond best to textures, image “styles”, and other regional “grouped” visual elements. We label neural NR-IQA models, such as MUSIQ, as high-level, as they process the image holistically, taking semantic context into account, as well as aesthetics, though they may also care about low-level issues, such as noise and blur. In general, including in our work, low-level metrics tend to measure distortion, while mid-level and high-level ones are more related to perceptual quality. However, there may be exceptions: for instance, measuring sharpness via a simple image filter is a low-level NR metric that targets perceptual quality rather than distortion (e.g., [78]).

14. Limitations

While our IQA-based method is able to sharpen SR outputs, as well as hallucinate aesthetically pleasing details in most cases, there are still several shortcomings to our approach. First, higher IQA model score does not guarantee improved human perceptual quality nor does it strictly ensure our outputs are artifact-free. This is related to the discussion in §4.3 and Fig. 3, where we postulate that some image changes can improve IQA score despite worsening perceptual quality (e.g., direct optimization being similar to an adversarial attack on the quality model). In Fig. 8, row two, for instance, we see that the SR model fails to predict the correct image details, leading to incorrect line orientations and aliasing-like artifacts (though the UPos baseline in column two arguably has worse artifacts). Second, from a semantic perspective, certain classes of image content may require different treatment, the requirements of which NR-IQA models are not naturally aware. For example, row one in Fig. 8 demonstrates how super-resolved *text* can become mangled. In terms of human preference, it can be argued that having a blurrier output in such uncertain cases may be more desirable (i.e., having blurred characters, rather than *wrong* characters, could be preferred for text). Nevertheless, text is notoriously challenging to super-resolve (prompting development of specialized methods for it [49, 103]); further, the UPos baseline suffers from similar artifacts as our outputs. Overall, we suspect better IQA models or more so-



Figure 8. **Illustration of limitations.** We show examples of shortcomings of our method (see Fig. 14), with MUSIQ scores in insets. In row one, we show the shortcomings of our model with respect to text, a particularly difficult form of image content. In row two, we see that our model does still incur artifacts, such as the mangled lines in the zoomed inset.

phisticated regularized optimizations (i.e., beyond LoRA) can mitigate some of the artifacts incurred by our approach. Handling more semantic issues, such as text hallucination, may require more specialized models.